ISIJ International, Vol. 58 (2018), No. 2, pp. 259–266

Thermodynamic Modeling of the SFCA Phase $Ca_2(Fe,Ca)_6(Fe,Al,Si)_6O_{20}$

Reiko MURAO,[1)]* Takayuki HARANO,[1)] Masao KIMURA[2,3)] and In-Ho JUNG[4)]

1) Advanced Technology Research Laboratories, Nippon Steel and Sumitomo Metal Corp., 20-1 Shintomi, Futtsu, Chiba, 293-8511 Japan.
2) Photon Factory, Institute of Materials Structure Science, High Energy Accelerator Research Organization, 1-1 Oho, Tsukuba, Ibaraki, 305-0801 Japan.
3) Department of Materials Structure Science, School of High Energy Accelerator Science, SOKENDAI (The Graduate University for Advanced Studies), 1-1 Oho, Tsukuba, Ibaraki, 305-0801 Japan.
4) Mining and Materials Engineering, McGill University. Now at Department of Materials Science and Engineering, College of Engineering, Seoul National University, 1 Gwanak-ro, Gwanak-gu, Seoul, 08826 South Korea.

(*Received on August 8, 2017; accepted on October 10, 2017*)

The thermodynamic model of a silico-ferrites of calcium and aluminum solution, SFCA phase ($Ca_2(Fe,Ca)_6^{Oct}(Fe,Al,Si)_6^{Tet}O_{20}$) was newly developed in the framework of the Compound Energy Formalism (CEF). Preferred substitution of Al atoms to tetrahedral sites in the SFCA solution was verified by X-ray absorption near edge structure (XANES) analysis. On considering crystallographic information in particular the short-range-ordering nature in the SFCA solution, the $Ca_8(Fe^{3+})_2^{Oct}(CaSi^{6+},FeFe^{6+},FeAl^{6+})_3^{Paired}(CaSi^{6+})_1^{Paired}(Fe^{3+},Al^{3+})_{20}^{Tet}O_{80}$ structure was considered for modeling the SFCA solution. The optimized Gibbs energies of all end-members can successfully reproduce the experimental single phase region of the SFCA solution.

KEY WORDS: iron ore sinter; calcium-ferrite; thermodynamic model.

1. Introduction

Sinter ore is the main iron burden of the iron-making process in Asia-Pacific region. In the industrial sintering process, the fine ores are mixed with limestone flux and coke breeze, and heated by the combustion of coke breeze at a temperature range of 1 450–1 600 K (above the eutectic temperature of the $CaO–Fe_2O_3$ system at 1 478 K) for a few minutes. The consolidation of iron ore grains progresses with the formation of the Ca–Fe–O melt and material transportation through the melt, and is hence called liquid-phase sintering.[1–5)] The micro-texture of the sinter basically comprises the iron ore grains, bonding, pores, and cracks. The matrix of the bonding phases which precipitated from the Ca–Fe–O melt are composed of the calcium ferrites ($CaO–Fe_2O_3$), silico-ferrites of calcium and aluminum, secondary hematite, magnetite, silicate glass ($CaO–SiO_2$), and their solid-solution phases, and these play an important role to give appropriate sinter properties such as strength and reducibility.[1)] The quantity of liquid formed during sintering process is affected by various process factors such as heat pattern, the composition of sinter and oxygen pressure near grain boundary of iron ore grains. Although the sintering reaction is a non-equilibrium and inhomogeneous, it is important to understand solid–liquid equilibrium of the sinter ore system for the quantitative analysis and verification of these factors.

A quasi-binary system such as $Fe_2O_3–CaO$ has been experimentally well analyzed.[6)] However, there are still unclear regions in the multi-component system consists high FeO_x and gangue mineral components such as SiO_2 and MgO. The quasi-ternary $CaO–Fe_2O_3–SiO_2$ system was experimentally studied by Kimura *et al.* under various oxygen partial pressures ranging from ambient to 10^{-3} Pa.[7)] As for the high Fe_2O_3 region of the $Al_2O_3–CaO–Fe_2O_3$ system around 1 573 K, the latest report was in 1967,[8)] which presented many ternary solid phases. The liquid region of the quasi-quaternary $Al_2O_3–CaO–Fe_2O_3–SiO_2$ system was only researched around 5 mass% Al_2O_3. In the $Al_2O_3–CaO–Fe_2O_3–SiO_2$ system, several large solid solutions of the silico-ferrites of calcium and aluminum are formed. There are at least three types of silico-ferrites of calcium and aluminum, the so-called SFCA ($A_2T_6M_6O_{20}$), SFCA-I ($A_3BM_8T_8O_{28}$) and SFCA-II ($A_4T_{14}M_{16}O_{48}$) phases, which are homologous series based on that of aenigmatite.[9–13)] In the structure formula, $A = Ca^{2+}$, $B = Ca^{2+}$ and Fe^{2+}, and M and T indicate the octahedral and the tetrahedral cation sites, respectively. The stable regions of these phases were experimentally researched by Patrick and Pownceby, but had not been completely clarified yet, as shown in **Fig. 1**.[14)] The homogeneity range of the SFCA-I and SFCA-II phases are still under discussion. The Si-free SFCA-II is a ternary solid solution of $CaO·3(Fe,Al)_2O_3$ with a compositional range of Fe_2O_3 between 44.5 and 81.5 mol%, according to Dayal and Glasser.[8,15)] Patrick and Pownceby also reported possibility

* Corresponding author: E-mail: murao.5gg.reiko@jp.nssmc.com
DOI: http://dx.doi.org/10.2355/isijinternational.ISIJINT-2017-459

of substitution of the SFCA-I and SFCA-II phases.[14)]

The crystal structures of the SFCA, SFCA-I and SFCA-II phases can be described as the sequences of pyroxene (*P*) and spinel (*S*) modules. The SFCA phase has the *P*-*S*-*P*-*S*- cycle, and its composition is a high-Si and low-Fe type with a wide range of Al substitution. The SFCA-I phase has the *P*-*S*-*S*-*P*-*S*-*S*- cycle and its composition is a low-Si and high-Fe type compared to the SFCA phase.[11)] The structure of the Si-free SFCA-II was determined by the single crystal X-ray diffraction analysis, and its structure indicated the features of both SFCA and SFCA-I type, resulting in the *P*-*S*-*P*-*S*-*S*- cycle.[12)]

In the case of a multi-component system, it is quite difficult to clarify all the complex phase equilibria between solids and liquid phases under different partial pressure of oxygen. Therefore, the CALPHAD type thermodynamic database, which is constructed based on the critical evaluation and optimization of all the reliable thermodynamic and phase diagram data in the literature, can be a very useful tool to identify complex phase equilibrium at the composition and partial pressure condition of interest. The FactSage thermodynamic database[16,17)] has been built for the past several decades and widely applied to the pyrometallurgical processes including ironmaking and steelmaking.[18)] Regarding the Al_2O_3–CaO–Fe_2O_3–SiO_2 system—in particular for iron sinter ore application, however— the SFCA phase which is one of the key sinter phases is missing in the database.

The aim of this study is to propose a thermodynamic model of the SFCA solution phase in the Al_2O_3–CaO–Fe_2O_3–SiO_2 system. To well describe the thermodynamic nature of the SFCA phase, the crystal structure of the SFCA phase should be taken into account in the CALPHAD-type modeling. Although the crystal structure of the SFCA had been already determined via single X-ray diffraction analysis,[11)] the distribution of Al was unclear especially for high-Al-bearing SFCA phase. Therefore, in the present study, X-ray absorption near edge structure (XANES) of Al and Fe was also investigated to analyze the coordination environment of cation. The thermodynamic model parameters of the SFCA phase were optimized to reproduce the liquid- and solid-phase equilibria related to the SFCA phase in the Al_2O_3–CaO–Fe_2O_3–SiO_2 system in air. The FactSage 6.4 FToxid database was used for all other solid and liquid phases in the quasi-quaternary system.

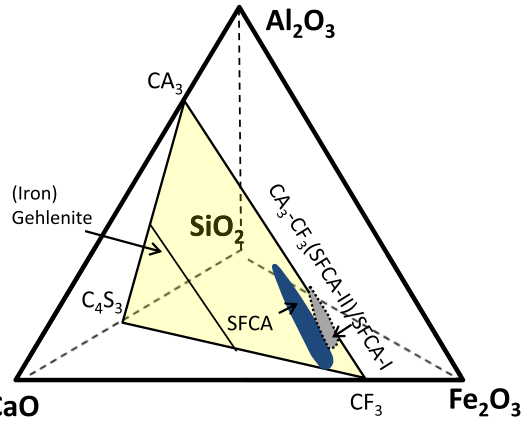

Fig. 1. (a) Schematic phase diagram indicating the $CaAl_6O_{10}$–$Ca_4Si_3O_{10}$–$CaFe_6O_{10}$ (CA3–C4S3–CF3) plane, the SFCA single phase region determined by experiments[14)] and possible region of CA_3–CF_3(SFCA-II)/SFCA-I substitution in the Al_2O_3–CaO–Fe_2O_3–SiO_2 system. (Online version in color.)

2. Experimental and Thermodynamic Calculations

2.1. Sample Preparation

Three SFCA samples with different compositions were prepared by the conventional powder sintering method for X-ray absorption measurements. Starting materials, α-Fe_2O_3 (4N grade, 1 μm), $CaCO_3$ (4N grade, 12 μm), α-SiO_2 (99%, 1 μm) and α-Al_2O_3 (4N grade, 1 μm), were mixed with an agate pestle and a mortar with the nominal compositions shown in **Table 1**. 1 g of each sample was pressed into pellets having a diameter of 13 mm at a pressure of 24 MPa. These pellets were calcined at 1 070 K for 10 h for decarbonation, then crushed, pelletized, and sintered at 1 500 K over 60 h in a platinum crucible. Products were confirmed as single phases of SFCA by powder X-ray diffraction measurements and those compositions were checked via X-ray fluorescent analysis.

Reference material $FePO_4$ was prepared by dehydration of $FePO_4 \cdot 8H_2O$ at 870 K. $Ca_2Fe_2O_5$, $CaFe_2O_4$, $Ca_2(Fe,Al)_2O_5$ were prepared by the same process of SFCA, but the sintering temperature was 1 370 K.

2.2. X-ray Absorption Measurements

XAFS experiments were conducted at Photon Factory, KEK (KEK-PF), Japan. Al *K*-edge XANES spectra were collected at BL-11A, KEK-PF, by total electric yield (TEY). Powdered samples were dispersed on the carbon conductive tape and put in the vacuum chamber with pressure under 10^{-6} torr. The incident X-ray energy from a bending-magnet source was scanned at 0.1 eV steps by rotating a grazing-incidence monochromator. The groove density of the grating was 1 200 lines/mm. X-ray beam size is 2 mm^V × 5 mm^H. The incident X-ray intensity and the sample current were measured for TEY. The energy scale was calibrated at $1s \rightarrow t_{1u}$ peak top of Al *K*-edge absorption of α-Al_2O_3 as 1 568.7 eV.

Fe *K*-edge XANES spectra were collected at BL-9A by transmitting method at energy steps of 0.35 eV, with a beam size of 1 mm^V × 1 mm^H. The incident X-ray energy was scanned by rotating the Si(111) double-crystal monochromator. The monochromator was detuned (rotated off the Bragg condition) 20% down for eliminating the high harmonic waves. A 170-mm-long ion chamber was used for measuring the incident X-ray intensity and a 310-mm-long ion chamber was used for measuring the transmitted intensity. The energy scale was calibrated at the minimum point of 1st differential curve of *K*-edge absorption of Fe foil as 7 113.2 eV. Normalized XANES data ($\Delta\mu t$ = 1) were used to calculate the integrated intensity of pre-edge peak of Fe

Table 1. Chemical composition of sintered SFCA (mol%).

Sample	Fe_2O_3	CaO	Al_2O_3	SiO_2
SFCA05	56.1	30.4	5.7	7.9
SFCA15	50.4	27.3	17.1	5.2
SFCA30	37.2	25.8	32.2	4.9

K-edge. Synthesized SFCA and reference materials were ground into powder with 10 μm diameter and diluted with BN powder for the X-ray absorption measurements.

2.3. FactSage Thermodynamic Databases

Phase equilibrium calculations of the Al_2O_3–CaO–Fe_2O_3–SiO_2 system were conducted by using thermodynamic database with Gibbs energy minimization software, FactSage 6.4. FactSage FToxid database was used for various solid and liquid oxide phases, and FACTPS (pure substances database) was used for gas phases to fix the oxygen partial pressure.

The Modified Quasi-chemical Model (MQM) is used in the FToxid database for the multi-component molten oxide solution.[19,20] The MQM can reproduce the oxygen bonding structure in molten oxide. For example, the network breaking reaction of SiO_2 by network modifier (MO) can be well reproduced in the MQM by the (Si–O–Si) + (M–O–M) = 2 (Si–O–M) pair exchange reaction between second nearest cations, which is key to reproduce the entropy of mixing. Many binary and ternary liquid solutions have been modeled using the MQM and the Gibbs energies of the liquid solutions in higher-order systems are properly predicted from the model parameters of their sub-systems.

The Compound Energy Formalism (CEF)[21,22] has been used to describe complex solid solutions. In the CEF, the crystallographic information, in particular, the mixing of cations (species), at a given sublattice is properly taken into account for better reproduction of entropy of solid solution. In this study, the SFCA phase was newly modeled in the framework of the CEF with taking into account its crystallographic features.

All thermodynamic calculations in this study were performed using the FactSage software 6.4 version.

3. Results and Discussion

3.1. XANES Analysis

Figure 2 shows the normalized Al *K*-edge XANES spectra of the SFCA and reference materials, $AlPO_4$, α-Al_2O_3, $MgAl_2O_4$, $Al_4Si_4O_{10}(OH)_8$ and $Ca_2(Fe,Al)_2O_5$. Each SFCA specimen and $Ca_2(Fe,Al)_2O_5$ indicate pre-edge peak characteristics of Al in tetrahedral coordination at 1 563.5 eV. It could not be directly determined whether Al is distributed in the octahedral sites from these spectra without a simulation of multiple scattering, which was due to the broad shoulder observed around 1 575 to 1 567 eV.

Figure 3 shows the normalized Fe *K*-edge XANES spectra of the SFCA and reference materials. Pre-edge peaks due to 1*s* to 3*d* forbidden transition were observed around an energy of 7 108 eV and those energy positions were almost same among the SFCA and references containing Fe^{3+}. It is known that the energy position of the pre-edge peak of Fe *K*-edge absorption depends on the valence of iron ion and its peak intensity is stronger in the case of tetrahedral coordination with lower symmetry than octahedral coordination with higher symmetry.[23]

In the case of powder sintering in an air atmosphere, the SFCA with low Fe^{2+}/Fe^{3+} ratio such as 0.02 was formed[14] so that presence of Fe^{2+} could be ignored. The peak profile of pre-edge was fitted by the Gaussian function after spline

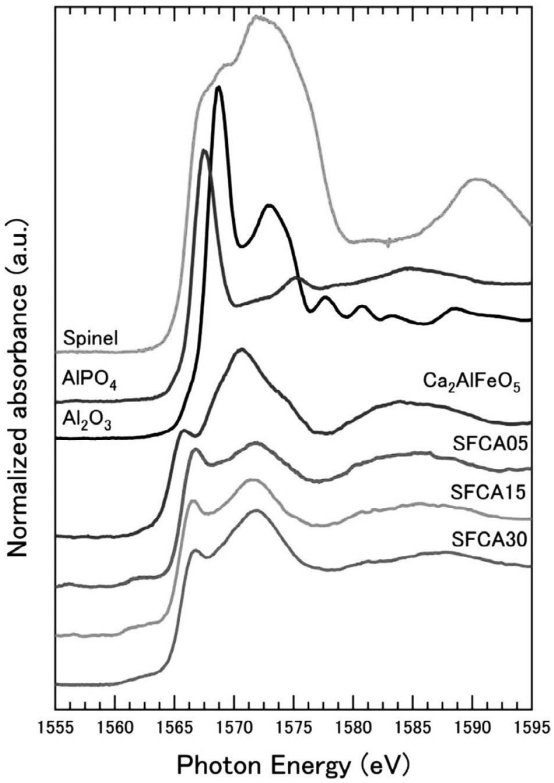

Fig. 2. Al *K*-edge XANES spectra of spinel, $AlPO_4$, Al_2O_3, $Ca(Fe_{0.5}Al_{0.5})_2O_5$, SFCA05, SFCA15 and SFCA30.

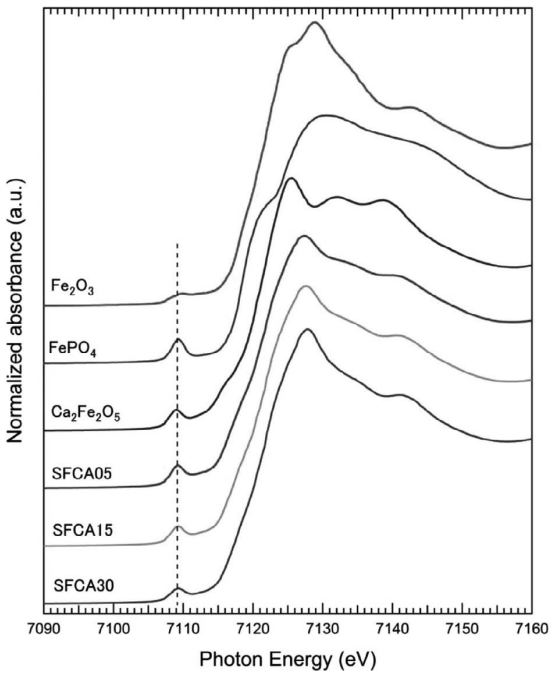

Fig. 3. Fe *K*-edge XANES spectra of Fe_2O_3, $FePO_4$, $Ca_2(Fe_{0.5}Al_{0.5})_2O_5$, SFCA05, SFCA15 and SFCA30. Dashed line indicates the pre-edge peak position.

fitting of the base line and integrated peak intensity was obtained. **Figure 4**(a) shows the pre-edge peak height of normalized Fe *K*-edge XANES spectra for each specimen. The pre-edge intensity of $FePO_4$, which has one tetrahedral-coordinated site of Fe, was the highest among specimens. The lowest peak intensity was obtained for those of $CaFe_2O_4$ and α-Fe_2O_3, which have only octahedral-coordinated sites of Fe. $Ca_2Fe_2O_5$ has one octahedral- and one tetrahedral-

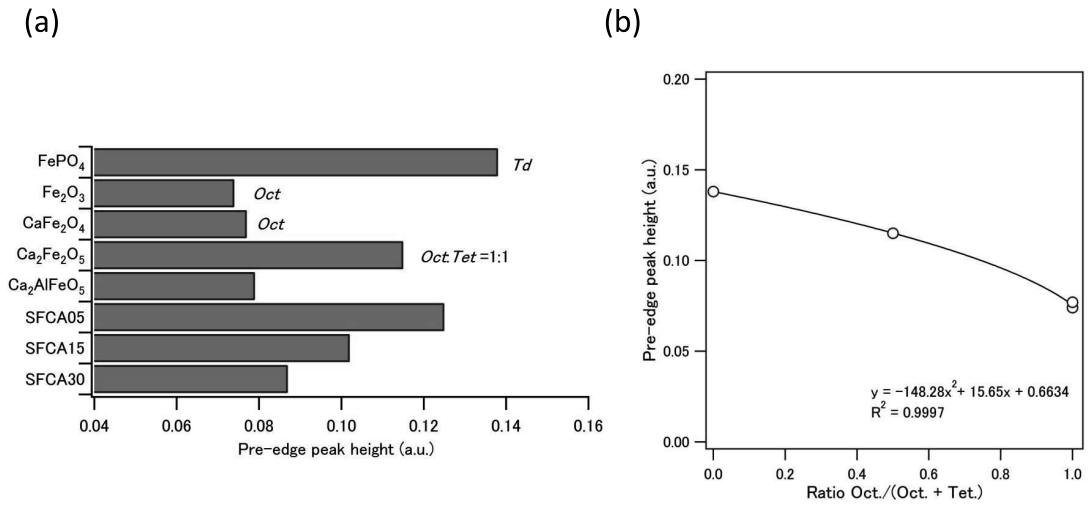

Fig. 4. (a) The pre-edge peak height of pre-edge peak of $FePO_4$, Fe_2O_3, $CaFe_2O_4$, $Ca_2Fe_2O_5$, $Ca_2(Fe_{0.5}Al_{0.5})_2O_5$, SFCA05, SFCA15 and SFCA30. (b) Relation between the atomic ratio of iron in octahedral site to total (octahedral + tetrahedral) iron and the pre-edge peak height of normalized Fe *K*-edge XANES spectra.

Table 2. Distribution of cations in octahedral and tetrahedral sites and distribution of Fe determined via Fe *K*-edge XANES analysis.

Sample	Site occupancy of cation (a.p.f.u.)							Ratio of Fe^{3+}	
	Octahedral sites			Tetrahedral sites			Total	Oct/(Oct+Tet)	
	Ca^{2+}	Fe^{3+}	Al^{3+} (fixed)	Fe^{3+}	Si^{4+}	Al^{3+}	Fe^{3+}	Calcd.	XANES
SFCA05	0.67	5.33	0	4.34	0.67	0.99	9.66	0.55	0.30
SFCA15	0.43	5.57	0	2.75	0.43	2.83	8.32	0.67	0.72
SFCA30	0.39	5.61	0	0.40	0.39	5.21	6.00	0.93	0.90
$Ca_2(Fe,Al)_2O_5$	–	1	0	0	–	1	1	1	0.97

coordinated site, so that the pre-edge intensity was at middle among the references materials. The SFCA structure has six tetrahedral-coordinated cation sites and six octahedral-coordinated cation sites. Fe atoms are distributed in both sites, while Si atoms occupy only tetrahedral sites. Ca atoms are distributed in two 7-coordinated sites and octahedral sites. On the contrary, Al is amphoteric and is possibly distributed in both tetrahedral and octahedral sites, but it may depend on the coordination environment of each site such as cation–oxygen distances. To determine the distribution of Al in octahedral and tetrahedral sites in the SFCA structure, a quadratic correlation equation between the ratio of Fe occupying the octahedral sites to the total Fe and integrated pre-edge peak intensity was made from the data set of $FePO_4$, $Ca_2Fe_2O_5$, $CaFe_2O_4$, and α-Fe_2O_3, as shown in Fig. 4(a). As a result of determination of distribution of Fe, that of Al in octahedral and tetrahedral sites could be conducted.

Table 2 shows the calculated distribution of cations (a.p.f.u.) in the octahedral and tetrahedral sites of the SFCA and the ratio of octahedral site occupancy of Fe, assuming all Al atoms to be in tetrahedral sites. The right column shows the ratio of octahedral site occupancy of Fe determined via XANES pre-edge peak intensity analysis. The XANES analysis results well agreed with the assumption of preferred substitution of Al in tetrahedral sites. In the case of SFCA30, which is at the almost maximum limit of Al solid solution-range, most of Fe is distributed in octahedral sites, which means the compositional range of SFCA phase is limited by the substitution limit of Al in the tetrahedral site.

As a result of the XANES analysis, the SFCA solid solution can be described as $Ca_2(Fe,Ca)_6^{Oct}(Fe,Al,Si)_6^{Tet}O_{20}$.

3.2. Thermodynamic Modeling of SFCA

The thermodynamic model of the SFCA solution was developed in the framework of the CEF. Several sublattice structures were tested for describing the SFCA solution. As the thermodynamic properties of the SFCA solution have not been determined, the model was verified to reproduce the phase equilibria between liquid and SFCA by Patrick and Pownceby.[14)]

The Gibbs energy of an oxide solid solution can be described by the CEF considering its crystallographic nature. Let's assume the crystal structure of the solution, $A_a(X,Y)_m^O(M,N)_n^TO_z$, where a, m, n and z represent the number of sublattices per formula unit. X and Y cations can occupy "O" sublattices and M and N cations can do "T" sublattices. Then, the Gibbs energy of this solid solution per formula can be described as follows using the CEF:

$$G^m = \sum_i \sum_j Y_i^O Y_j^T G_{ij} - TS_c + G^E \quad \text{..... (1)}$$

$$S_c = -R\left(m\sum_i Y_i^O \ln Y_i^O + n\sum_j Y_j^T \ln Y_j^T\right) \quad \text{..... (2),}$$

where Y_i^O and Y_j^T are site fraction of i and j cations in the "O" and "T" sites. G_{ij} represents the molar Gibbs energy of

$A_a(i)_m^O(j)_n^T O_z$ end-member of the solution. S_c is the configuration entropy of solution which is calculated based on the random mixing of species at O and T sublattices, where m and n are the number of moles of the O and T sublattices, respectively. That is, the CEF considers the random mixing of species at a given sublattice. G^E is the excess Gibbs energy, which includes the interaction energy between the mixing species in the solution. The main model parameters in the CEF are the Gibbs energy of end-member, G_{ij}. In particular, as some of the end-members in the Gibbs energy description can be imaginary pseudo-components, their Gibbs energy values can directly influence to the Gibbs energy of solution. If necessary, G^E can be introduced to further refine the Gibbs energy of the solution.

The most simplest and straightforward sublattice structure of the SFCA phase we can think about is

$$Ca_2(Fe^{3+},Ca^{2+})_6^{Oct}(Fe^{3+},Al^{3+},Si^{4+})_6^{Tet}O_{20} \quad \cdots\cdots (3),$$

where only octahedral and tetrahedral sites are subject to mix the different cations. Then, the molar Gibbs energy, G^m, of the SFCA solution per formula can be described using the Eqs. (1) and (2). Under this formula, six end-members can be defined: $Ca_2(Ca)_6^{Oct}(Si)_6^{Tet}O_{20}$, $Ca_2(Fe)_6^{Oct}(Fe)_6^{Tet}O_{20}$, $Ca_2(Fe)_6^{Oct}(Al)_6^{Tet}O_{20}$, $Ca_2(Fe)_6^{Oct}(Si)_6^{Tet}O_{20}^{6+}$, $Ca_2(Ca)_6^{Oct}(Fe)_6^{Tet}O_{20}^{6-}$, and $Ca_2(Ca)_6^{Oct}(Al)_6^{Tet}O_{20}^{6-}$. Among them, the first three neutral end-members correspond to the composition of $Ca_4Si_3O_{10}$, $CaFe_6O_{10}$, and $CaFe_3Al_3O_{10}$, in the phase diagram of the $Ca_4Si_3O_{10}$–$CaFe_6O_{10}$–$CaAl_6O_{10}$ system, as shown in Fig. 1 . The other 3-charged end-members are not in the section of the section. Using this formula, it was very difficult to obtain the homogeneity range of SFCA solid solution up to 35 mol% of $CaAl_6O_{10}$ in the $Ca_4Si_3O_{10}$–$CaFe_6O_{10}$–$CaAl_6O_{10}$ system. The only way to increase the homogeneity range toward $CaAl_6O_{10}$ was to stabilize the pseudo-end member $Ca_2(Fe)_6^{Oct}(Al)_6^{Tet}O_{20}$ by decreasing its Gibbs energy. However, this would cause the formation of stable $CaFe_3Al_3O_{10}$ in the $CaFe_6O_{10}$–$CaAl_6O_{10}$ section. In addition, it was difficult to control the solubility of Si in SFCA structure within the experimentally measured concentration range (Si = 0.25–1.0 mole per mole of $Ca_2(X)_6^{Oct}(Y)_6^{Tet}O_{20}$),[12] which was mainly by the Gibbs energy of $Ca_2(Ca)_6^{Oct}(Si)_6^{Tet}O_{20}$.

There is a charge compensation relationship, $(Ca^{2+})^{Oct}$ + $(Si^{4+})^{Tet}$ = $(Fe^{3+})^{Oct}$ + $(Fe^{3+}, Al^{3+})^{Tet}$ in the SFCA structure. That is, when Si^{4+} dissolves in tetrahedral sites with the replacement of Fe^{3+} or Al^{3+}, Ca^{2+} should be dissolved in the octahedral site by replacing Fe^{3+}. **Figure 5** shows the crystal structure of the SFCA phase based on the crystallographic data reported by Hamilton *et al.*[10] As can be seen, Si^{4+} was concentrated at a certain tetrahedral site and was located close to the octahedral site concentrated by Ca^{2+}, rather than the occupation of Si^{4+} and Ca^{2+} occur randomly in octahedral and tetrahedral sites, respectively. This means that the sublattice structure used in the above SFCA model is improper and can overestimate the entropy of mixing of real solution.

To describe such a short-range-ordering behavior between Si^{4+} and Ca^{2+} in the SFCA structure, a pair of the tetrahedral and the octahedral sites can be considered as one of the sublattices. As the concentration range of Si in air atmosphere ranges between 0.25 and 1.0 atom per six tetrahedral-coordinate sites[13] (that is, the maximum number of Si occupancy in tetrahedral sites is 1 out of 6), 1/6 of the tetrahedral and the octahedral sites were considered as the paired sites. In the paired sites, CaSi, FeFe and FeAl pairs can exist assuming the cation species in the octahedral and the tetrahedral sites (Ca and Fe in octahedral sites and Fe, Al, and Si in tetrahedral sites). In particular, no CaFe, CaAl and FeSi pairs were considered in the paired sites to make sure that all Ca are paired with Si and vice versa. There is one mole of paired sites per mole of SFCA solution with $Ca_2(X)_6^{Oct}(Y)_6^{Tet}O_{20}$ formula. Among one mole of paired sites, a quarter of them were again assigned only for CaSi in order to intentionally make sure that solubility of Si in SFCA can vary from 0.25 mole per mole of $Ca_2(X)_6^{Oct}(Y)_6^{Tet}O_{20}$. The rest of the octahedral sites were assumed to be occupied only by Fe, and the rest of the tetrahedral sites were occupied by Fe and Al. In summary, the revised crystal structure of the SFCA phase is as follows:

$$Ca_8(Fe^{3+})_{20}^{Oct}(CaSi^{6+},FeFe^{6+},FeAl^{6+})_3^{Paired}(CaSi^{6+})_1^{Paired}(Fe^{3+},Al^{3+})_{20}^{Tet}O_{80} \quad \cdots\cdots (4),$$

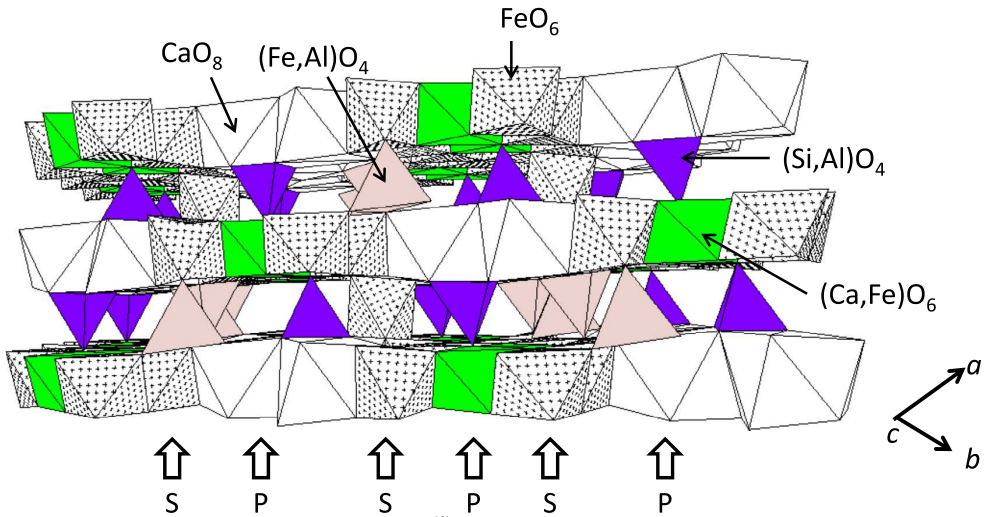

Fig. 5. Schematic of the crystal structure of SFCA[10] indicating spinel (*S*) and pyroxene (*P*) modules, and the short-range-ordering of Si and Ca in tetrahedral $(Si,Al)O_4$ sites and octahedral $(Ca,Fe)O_6$ sites, respectively. (Online version in color.)

which is presented per mole of $Ca_8(X)_{24}^{Oct}(Y)_{24}^{Tet}O_{80}$.

There are six end-members to describe the revised SFCA solution with the above-mentioned crystal structure using the CEF. **Figure 6**(a) shows a schematic illustration of the end-members in the bi-pyramid structure, and Fig. 6(b) shows the compositions of the end-members projected on the $CaAl_6O_{10}$–$Ca_4Si_3O_{10}$–$CaFe_6O_{10}$ (CA3–C4S3–CF3) plane. In Fig. 6(b), circle and triangle symbols indicate single-phase SFCA region that was experimentally confirmed.[13,14] It should be noted that the compositional range of the end-members in the SFCA solution is wide enough to contain all the experimental single-phase SFCA compositions, and all the end-members are charged neutral.

In the formula of the SFCA solution in Eq. (4) , let us assign 3 moles of paired sites containing CaSi, FeFe, and FeAl as P sites, and 20 moles of tetrahedral sites containing Fe and Al as the T site for the simplicity. According to the Eqs. (1) and (2), the molar Gibbs energy of the SFCA solution per mole of $Ca_8(X)_{24}^{Oct}(Y)_{24}^{Tet}O_{80}$ can be expressed as follows:

$$G^m = \sum_i \sum_j Y_i^P Y_j^T G_{ij} - TS_c + G^E \quad \text{..... (5)}$$

$$S_c = -R\left(3\sum_i Y_i^P \ln Y_i^P + 20\sum_j Y_j^T \ln Y_j^T\right) \quad \text{..... (6)},$$

where Y_i^P and Y_j^T are occupancy of i or j cation in the P and T site, respectively, and G_{ij} is the molar Gibbs energy of end member $Ca_8(Fe^{3+})_{20}^{Oct}(i)_3^{Paired}(CaSi^{6+})_1^{Paired}(j)_{20}^{Tet}O_{80}$. The configuration entropy, S_c, is also defined as shown in Eq. (6).

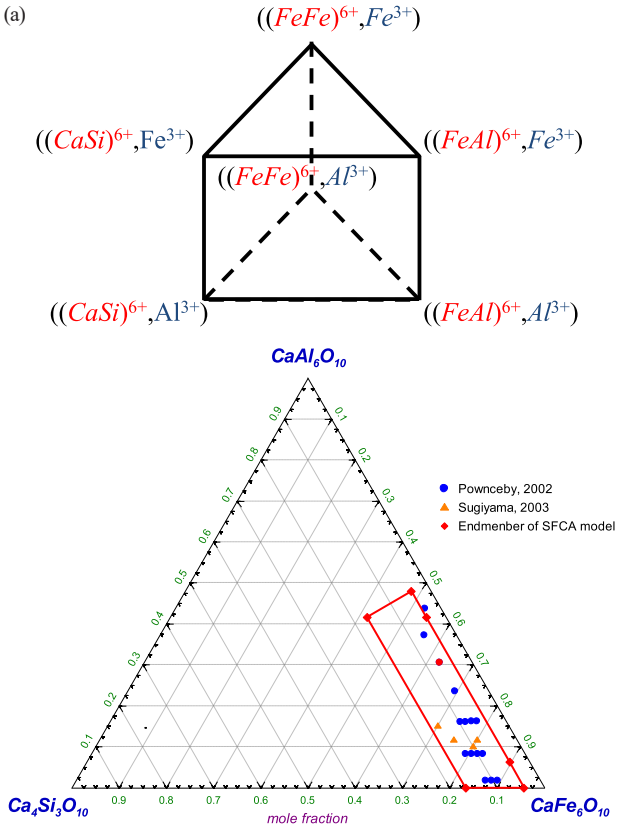

Fig. 6. (a) Schematic of the Gibbs energy of end-members of SFCA solution, and (b) the compositions of six end-members of the SFCA solution model on the $CaAl_6O_{10}$–$Ca_4Si_3O_{10}$–$CaFe_6O_{10}$ (CA3–C4S3–CF3) plane. Circle and triangle symbols indicate the composition of single phase SFCA that were experimentally determined.[13,14] (Online version in color.)

In the description of solution using the CEF, the molar Gibbs energy of six end-members G_{ij} are the most important model parameters. None of G_{ij} in the present formula is the actual stable phase in the $CaAl_6O_{10}$–$Ca_4Si_3O_{10}$–$CaFe_6O_{10}$ system. Therefore, logical determination of G_{ij} is essential to accurately describe the Gibbs energy of the SFCA solution. In the present study, G_{ij} (in the following expression, it is presented as $G^o(i^P j^T)$) were defined using the well-known molar Gibbs energies of stable compounds such as $CaFe_4O_7$, $CaAl_4O_7$, $Ca_3Si_2O_7$, $CaSiO_3$, Fe_2O_3, and Al_2O_3:

$$G^o(\mathrm{CaSi}^P\mathrm{Fe}^T) = \frac{40}{6}G^o_{CF2} + \frac{8}{6}G^o_{C3S2} + \frac{8}{6}G^o_{CS} + \frac{40}{6}G^o_F + G_1 \quad \text{..... (7)}$$

$$G^o(\mathrm{CaSi}^P\mathrm{Al}^T) = \frac{20}{6}G^o_{CF2} + \frac{20}{6}G^o_{CA2} + \frac{8}{6}G^o_{C3S2} + \frac{8}{6}G^o_{CS} + \frac{20}{6}G^o_F + \frac{20}{6}G^o_A + G_2 \quad \text{... (8)}$$

$$G^o(\mathrm{FeFe}^P\mathrm{Fe}^T) = \frac{46}{6}G^o_{CF2} + \frac{2}{6}G^o_{C3S2} + \frac{2}{6}G^o_{CS} + \frac{46}{6}G^o_F + G_3 \quad \text{..... (9)}$$

$$G^o(\mathrm{FeFe}^P\mathrm{Al}^T) = \frac{26}{6}G^o_{CF2} + \frac{20}{6}G^o_{CA2} + \frac{2}{6}G^o_{C3S2} + \frac{2}{6}G^o_{CS} + \frac{26}{6}G^o_F + \frac{20}{6}G^o_A + G_4 \quad \text{... (10)}$$

$$G^o(\mathrm{FeAl}^P\mathrm{Fe}^T) = \frac{43}{6}G^o_{CF2} + \frac{3}{6}G^o_{CA2} + \frac{2}{6}G^o_{C3S2} + \frac{2}{6}G^o_{CS} + \frac{43}{6}G^o_F + \frac{3}{6}G^o_A + G_5 \quad \text{... (11)}$$

$$G^o(\mathrm{FeAl}^P\mathrm{Al}^T) = \frac{23}{6}G^o_{CF2} + \frac{23}{6}G^o_{CA2} + \frac{2}{6}G^o_{C3S2} + \frac{2}{6}G^o_{CS} + \frac{23}{6}G^o_F + \frac{23}{6}G^o_A + G_6 \quad \text{... (12)},$$

where G^o_{CF2}, G^o_{CA2}, G^o_{C3S2}, G^o_{CS}, G^o_F, and G^o_A are the molar Gibbs energy of $CaFe_4O_7$, $CaAl_4O_7$, $Ca_3Si_2O_7$, $CaSiO_3$, Fe_2O_3, and Al_2O_3, respectively. The expression of a given $G^o(i^P j^T)$ with stable compounds was chosen based on the number of each cation and anion in the individual end-member. G_1 to G_6 are the additional Gibbs energy terms to adjust the value of $G^o(i^P j^T)$.

In this study, G^E was set to be zero in Eq. (5). That is the Gibbs energy of the SFCA solution was fully described by the Gibbs energies of six end-members to reproduce the single SFCA phase region and associated phase equilibria with other phases.

3.3. Optimization of SFCA Thermodynamic Model

In this study, the G_1 to G_6 in Eqs. (7) to (12) were

optimized for the Gibbs energies of end-members of the SFCA solution model to reproduce an experimental data set reported by Patrick and Pownceby[14] in a temperature range between 1 513 and 1 663 K. **Table 3** shows the optimized values for G_1 to G_6 in this study. The isothermal phase diagrams of the CA3–CF3–C3S4 system in air atmosphere are calculated at 1 513, 1 543, 1 573 and 1 663 K as shown in **Figs. 7**(a) to 7(d) using the FToxid database and new SFCA solution model with the optimized parameters. The painted region in the figures shows the calculated SFCA single-phase region. Filled circles indicate experimental data points of single-phase SFCA and open circles indicate the mixtures of the SFCA and other phases by Patrick *et al.*[14] Filled triangles represent the mixtures of the SFCA and the meta-stable phase, possibly, due to low heating temperature and short heating period of sample preparations. Experimental homogeneity areas of the SFCA phase (single SFCA phase region) are successfully reproduced at temperatures between 1 543 and 1 663 K by the new SFCA model. At 1 513 K, the calculated SFCA single-phase at low Al region (>0.85CF3) is slightly inconsistent with experimental data; the calculated single-phase SFCA area in the low-CA3 region is more extended toward the CF3 corner than the experimental one. One possible reason to explain such inconsistency would be due to thermodynamic model of hematite phase used in these calculations, in which solid solution of CaO in Fe_2O_3 was not taken in considered.. In reality, Ca substitutes approximately 10% of Fe in hematite at 1 513 K to form Fe_2O_3-rich solid solution.[24] This would destabilize hematite phase and influence the single phase region of the SFCA phase. In addition, missing of SFCA-I phase model would also influence the stable region of the SFCA phase at around 0.85CF3.

Table 3. Optimized model parameters for the Gibbs energy of the end-member in the present SFCA model (kJ/mol).

G_1	G_2	G_3	G_4	G_5	G_6
−41.8	−347.3	−104.6	−836.8	−92.0	−418.4

The main focus of the present study is to develop the SFCA solution model using the CEF and optimize the model parameters. Although the SFCA region was successfully reproduced by using the present SFCA model, the other phases around the SFCA need to be assessed further. For this purpose, more studies dealing with the experimental phase diagram of the CA3—CF3—C3S4 system is also nec-

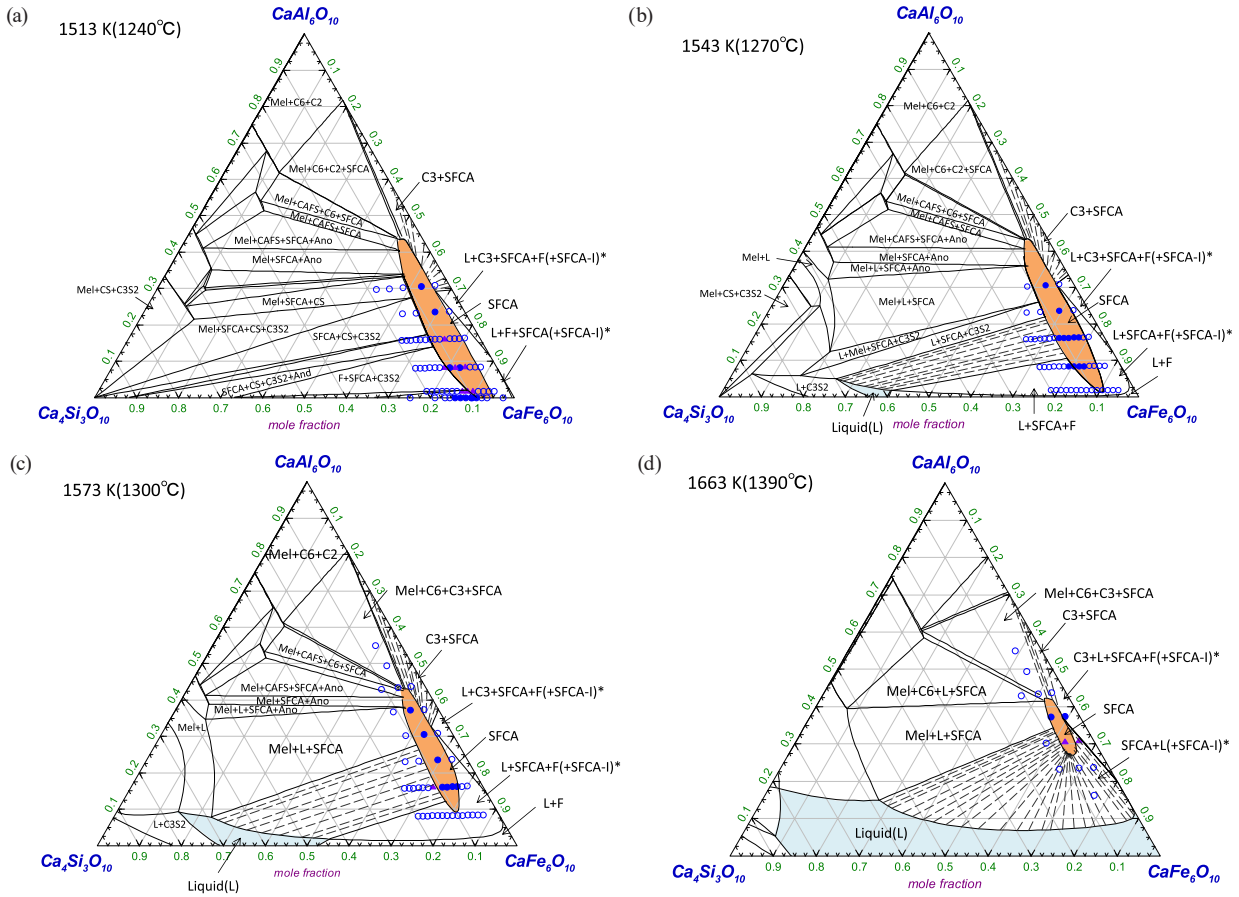

Fig. 7. Calculated isothermal phase diagrams of the CA3–CF3–C3S4 system using the present SFCA thermodynamic model at (a) 1 513 K, (b) 1 543 K, (c) 1 573 K and (d) 1 663 K, respectively. The painted regions show the calculated SFCA single-phase and liquidus region. Filled circles indicate experimental data points of single-phase SFCA, filled triangles represent the mixtures of the SFCA and the meta-stable phase and open circles indicate a mixture of SFCA and other phases reported by Patrick *et al.*[14] F, CS, C3S2, And, and Ano stand for the stoichiometric Fe_2O_3, $CaSiO_3$, $Ca_3Si_2O_7$, $Ca_3Fe_2Si_3O_{12}$, and $CaAl_2Si_2O_8$, respectively. Mel, CAFS, C6, C3, and C2 represent melilite, $Ca_2(Al,Fe)_8SiO_{16}$, $Ca(Al,Fe)_{12}O_{19}$, $Ca(Al,Fe)_6O_{10}$, and $Ca(Al,Fe)_4O_7$ solid solution, respectively. *Experimental data indicated the presence of SFCA-I, but the thermodynamic model of SFCA-I phase was not used in present calculations. (Online version in color.)

essary. Another multi-component calcium ferrites with the aenigmatite-type structure, SFCA-I, has not been modeled and the SFCA-II (*i.e.*, C3) with no SiO_2 should be optimized to explain the phase equilibria involving the SFCA phase in the low SiO_2 region. These will be further investigated in near future.

4. Conclusion

A new thermodynamic model of the SFCA phase was developed in this study. It was confirmed via XANES analysis that Al atoms in the SFCA solution prefer to substituting tetrahedral sites. Considering crystallographic information, in particular, the short-range-ordering nature in the SFCA solution, $Ca_8(Fe^{3+})_{20}^{Oct}(CaSi^{6+},FeFe^{6+},FeAl^{6+})_3^{Paired}(CaSi^{6+})_1^{Paired}(Fe^{3+},Al^{3+})_{20}^{Tet}O_{80}$ structure was considered for modeling the SFCA solution using the CEF. The optimized Gibbs energies of all end-members can successfully reproduce the single-phase region of the SFCA solution.

To analyze the real sintering process, the presence of Fe^{2+} or Mg^{2+} should be taken into consideration. It was reported that solution range of Si^{4+} and Ca^{2+} is increasing with increasing Mg^{2+} concentration.[13] Substitution of Fe^{2+} may increase in particular under low oxygen pressure. A further study on modeling different SFCA series will be required. The re-optimization of the $CaO–SiO_2–FeO–Fe_2O_3–Al_2O_3$ system in particular in the high-Fe-oxide region would be necessary to improve the description of the phase equilibration related to the iron ore sintering process.

Acknowledgement

X-ray absorption measurements were conducted under corroboration research between High Energy Accelerator Research Organization (KEK) and Nippon Steel & Sumitomo Metals Coop (Proposal No. 2015C206). The authors appreciated to Dr. Yoshinori Kitajima, KEK and Mr. Kengo Noami, Nippon Steel & Sumikin Technology Co., Ltd for their technical supports. The authors also thank Prof. Kazumasa Sugiyama of Tohoku Univ. for a fruitful discussion regarding the crystallographic characteristics of SFCA.

REFERENCES

1) T. Mukherjee and J. A. Whiteman: *Ironmaking Steelmaking*, **12** (1985), 151.
2) M. I. Pownceby, J. M. F. Clout and M. J. Fisher-White: *Trans. Inst. Min. Metall. Sect. C*, **107** (1998), No. 3, C1.
3) G. O. Egundebi and J. A. Whiteman: *Ironmaking Steelmaking*, **16** (1989), 379.
4) I. Ordavo, S. Ihle, V. Arkadiev, O. Scharf, H. Soltau, A. Bjeoumikhov, S. Bjeoumikhova, G. Buzanich, R. Gubzhokov, A. Günther, R. Hartmann, P. Holl, N. Kimmel, M. Kühbacher, M. Lang, N. Langhoff, A. Liebel, M. Radtke, U. Reinholz, H. Riesemeier, G. Schaller, F. Schopper, L. Strüder, C. Thamm and R. Wedell: *Nucl. Instrum. Methods Phys. Res. A*, **654** (2011), 250.
5) K. Ohno, T. Miki, Y. Sasaki and M. Hino: *Tetsu-to-Hagané*, **95** (2009), 821.
6) J. Gröbner, S. Delsante, N. Solak and V. Tomashik: Calcium – Iron – Oxygen: Datasheet from Landolt-Börnstein - Group IV, Physical Chemistry, Vol. 11D2: Iron Systems, Part 2, SpringerMaterials, ed. by G. Effenberg and S. Ilyenko, Springer-Verlag, Berlin, Heidelberg, (2008), DOI: 10.1007/978-3-540-74196-1_17.
7) H. Kimura, S. Endo, K. Yajima and F. Tsukihashi: *ISIJ Int.*, **44** (2004), 2040.
8) R. R. Dayal and F. P. Glasser: *Sci. Ceram.*, **3** (1967), 191.
9) K. Inoue and T. Ikeda: *Tetsu-to-Hagané*, **68** (1982), 2190.
10) J. D. G. Hamilton, B. F. Hoskins, W. G. Mumme, W. E. Borbidge and M. A. Montague: *N. Jb. Miner. Abh.*, **161** (1989), 1.
11) W. G. Mumme, J. M. F. Clout and R. W. Gable: *N. Jahrb. Mineral. Abh.*, **173** (1998), 93.
12) W. G. Mumme: *N. Jahrb. Mineral. Abh.*, **178** (2003), 307.
13) K. Sugiyama, A. Monkawa and T. Sugiyama: *ISIJ Int.*, **45** (2005), 560.
14) T. Patrick and M. Pownceby: *Metall. Mater. Trans. B*, **33** (2002), 79.
15) D. H. Lister and F. P. Glasser: *Trans. Br. Ceram. Soc.*, **66** (1967), 293.
16) C. W. Bale, P. Chartrand, S. A. Degterov, G. Eriksson, K. Hack, R. Ben Mahfoud, J. Melançon, A. D. Pelton and S. Petersen: *Calphad*, **26** (2002), 189.
17) S. Decterov, Y.-B. Kang and I.-H. Jung: *J. Phase Equilib. Diffus.*, **30** (2009), 443.
18) I.-H. Jung: *Calphad*, **34** (2010), 332.
19) A. D. Pelton, S. A. Degterov, G. Eriksson, C. Robelin and Y. Dessureault: *Metall. Mater. Trans. B*, **31** (2000), 651.
20) A. Pelton and P. Chartrand: *Metall. Mater. Trans. A*, **32** (2001), 1355.
21) M. Hillert: *J. Alloy. Compd.*, **320** (2001), 161.
22) M. Hillert, L. Kjellqvist, H. Mao, M. Selleby and B. Sundman: *Calphad*, **33** (2009), 227.
23) M. Wilke, F. Farges, P.-E. Petit, G. E. Brown and F. Martin: *Am. Mineral.*, **86** (2001), 714.
24) B. Bergman: *J. Am. Ceram. Soc.*, **69** (1986), 608.